Proceedings of GT2006
ASME Turbo Expo 2006: Power for Land, Sea and Air
May 8-11, 2006, Barcelona, Spain

GT2006-90214

UNSTEADY AERODYNAMIC BLADE EXCITATION AT THE STABILITY LIMIT AND DURING ROTATING STALL IN AN AXIAL COMPRESSOR

Ronald Mailach, Konrad Vogeler

Technische Universität Dresden
Institute for Fluid Mechanics
01062 Dresden, Germany
E-Mail: mailach@tus.mw.tu-dresden.de

ABSTRACT

The stable operating range of axial compressors is limited by the onset of rotating stall and surge. These flow conditions endanger the reliability of operation and have definitely to be avoided in compressors of gas turbines. However, there is still a need to improve the physical understanding of these flow phenomena to prevent them while utilizing the maximum available working potential of the compressor.

This paper discusses detailed experimental investigations of the rotating stall onset with the main emphasis on the aerodynamic blade excitation in the Dresden four-stage Low-Speed Research Compressor. The stall inception, which is triggered by modal waves, as well as the main flow features during rotating stall operation are discussed. To investigate the unsteady pressure distributions, both the rotor and the stator blades of the first stage were equipped with piezoresistive pressure transducers. Based on these measurements the unsteady blade pressure forces are calculated. Time-resolved results at the stability limit as well as during rotating stall are presented. For all operating conditions rotor-stator-interactions play an important role on the blade force excitation. Furthermore the role of the inertia driven momentum exchange at the stall cell boundaries on the aerodynamic blade force excitation is pointed out.

Keywords: axial compressor, unsteady aerodynamic blade force, rotating stall, modal waves, rotor-stator-interaction

1 INTRODUCTION

The stable operating range of axial compressors for low mass flow is limited by the rotating stall (RS) inception. This flow regime can trigger the formation of surge, particularly for high rotational speed and large downstream plenum. In gas turbines and jet engines these dangerous flow conditions must be avoided because of the excitation of high-amplitude vibrations and high thermal loading of the blades and other machine components, which can result in a reduction of fatigue life or even a destruction of these machine parts. In practice this is done by maintaining a surge margin, which can amount to 20-25% of the compressor pressure rise. As a consequence the attainable efficiency of the machine is strongly reduced. Therefore, several control mechanisms for extending the usable operating range of axial compressors were discussed within recent years. A potential practical application of such methods requires a further improvement of the physical understanding of the stall and surge inception and development process.

There are different flow patterns, which precede the RS inception. The first one is the modal wave stall inception (McDougall et al. [1]). Modal waves are a typical stall precursor in low-speed compressors but have also been observed in high-speed compressors (Day et al. [2], Höss et al. [3]). Often this flow disturbance occurs only a short time before exceeding the stability limit of the compressor. Modal waves are a long-lengthscale wavelike disturbance of the pressure and velocity field rotating around the circumference. The breakdown of the flow field at the stability limit is initiated in a velocity minimum of the modal wave.

The second pattern is a short-lengthscale disturbance, which is known as “spike”. It is a small cell of stalled flow, which in its initial phase is typically limited to the blade tip region of only one or a few blade passages. It grows within a few rotor revolutions to a full-span RS cell. Camp and Day [4] give a detailed overview of the recent work on these two stall inception patterns.

Other flow patterns, which can already be found in the stable operating range of compressors and can be regarded as precursors for full-span RS, are short-lengthscale multicell configurations. These flow conditions can especially appear in blade rows with higher loading, e.g. in the front stages of high-

speed compressors at part speed, in mis-staggered blade rows or in blade rows with relative large tip clearance. This is discussed in Mailach et al. [5], [6].

The stall inception process in the Dresden four-stage axial Low-Speed Research Compressor (Dresden LSRC) will be discussed in this paper. An important aspect for a reliable operation of the compressor is the aerodynamic blade excitation at operating points near the stability limit and especially for unstable flow conditions, where a clear difference to the design conditions can be expected. Within recent years an increasing number of both experimental and numerical investigations on unsteady aerodynamic blade forces in turbomachinery became available. A literature survey on this topic is given by Mailach et al. [7], [8]. However, to the best knowledge of the authors up to the present only stable operating points of compressors are discussed in open literature. Experimental data about unsteady aerodynamic blade pressure forces for unsteady flow conditions in compressors are not available yet.

The aim of this paper is therefore to gain insight into the complex physics of aerodynamic blade excitation for unsteady flow conditions in compressors. On the basis of the time-resolved pressure measurements on the rotor and stator blade rows the unsteady pressure forces of the blades are calculated. Results will be presented for the exceeding of the stability limit and the developing RS regime. The excited pressure forces are quantified and compared to the results for stable operating points, which are available from previous investigations of the authors [7], [8].

2 EXPERIMENTAL SETUP, DATA ACQUISITION AND POSTPROCESSING

The Dresden LSRC consists of four identical stages, which are preceded by an inlet guide vane (IGV) row. Table 1 gives a summary of the main design parameters while fig. 1 shows a sectional drawing of the compressor. The blading of the compressor was developed on the basis of the profiles of a middle stage of a high-pressure compressor of a gas turbine. More detailed descriptions of the compressor are given by Sauer et al. [9], Müller et al. [10] and Boos et al. [11].

For the experiments, described in this paper, the operating point of the compressor was shifted on the design speed line from a stable operating point towards RS onset by closing the throttle slowly. When the stability limit was exceeded, the compressor was operated during RS for a maximum of 10 seconds while keeping the throttle position unchanged.

A single rotor blade and a single stator blade were equipped with altogether 36 time-resolving piezoresistive pressure transducers (*Kulite LQ47*). To minimize the influence on the flow the sensors and the wires were fitted into the blade surfaces. They are equally distributed along the midspan on the pressure side (PS) and the suction side (SS). On both blades the sensors are positioned from 10% to 90% chord with steps of 10% chord. The leading edge and the trailing edge regions could not be equipped with pressure transducers without disturbing the flow noticeably. As an example the rotor blade is shown in fig. 2.

Tab. 1: Design parameters of Dresden LSRC

IGV + 4 identical stages	
Reynolds number, rotor inlet, MS, DP (related to rotor chord length)	$5.7 \cdot 10^5$
Mach number, rotor inlet, MS, DP	0.22
Design speed	1000 rpm
Mass flow, DP	25.35 kg/s
Mean flow coefficient, DP	0.553
Enthalpy coefficient Ψis, DP	0.794
Hub diameter	1260 mm
Hub to tip ratio	0.84
Axial gaps between all blade rows, MS	32 mm

	IGV	rotor	stator
Blade number	51	63	83
Chord length, MS	80 mm	110 mm	89 mm
Stagger angle, MS (vs. circumference)	82.8°	49.3°	64.0°
Solidity, MS	0.941	1.597	1.709

MS: midspan
DP: design point

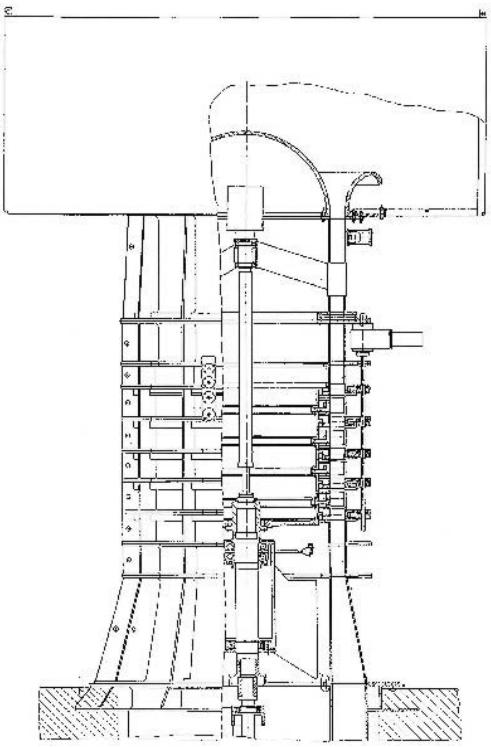

Fig. 1: Sectional drawing of Dresden LSRC

The investigations of the unsteady blade pressure forces at the stability limit and during rotating stall were performed on rotor 1 and stator 1, since the stall inception appears in the first stage. Both the steady and the unsteady part of the pressure were measured with the piezoresistive transducers. The zero point offset of the sensors was corrected before starting the short-duration measurements. The signals from the transducers were amplified 125 times. This was done using a separate miniature amplifier for each sensor. For the measurements on

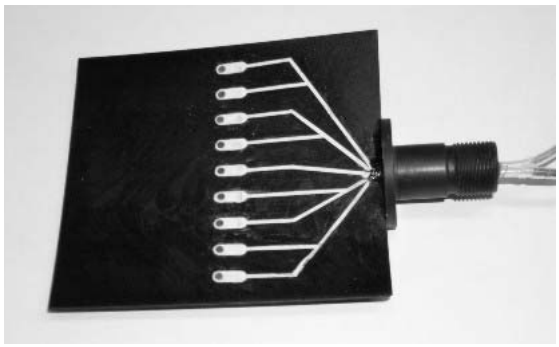

Fig. 2: Rotor blade equipped with piezoresistive pressure transducers on PS and SS (view on PS)

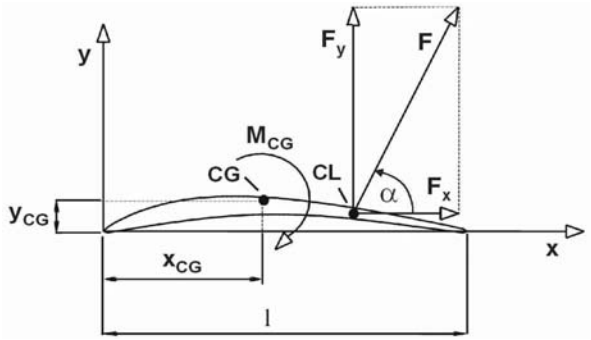

Fig. 3: Force definitions in blade coordinate system

the rotor blades the amplifier card was mounted within the rotor drum. The amplified signals are transmitted via slip rings into the fixed frame of reference.

The pressure force components F_x and F_y are referred to the blade coordinate system (fig. 3). They were calculated by integrating the measured unsteady pressure distributions along the PS and the SS with respect to the blade contour. The pressure in the leading edge and the trailing edge region was extrapolated to improve the accuracy of the results. Based on the time-resolved force components F_x and F_y further parameters were determined. These are the resulting pressure force F and the turning moment M_{CG}, which is referred to the centre of gravity (CG) of the blade. Eventually the angle α between the abscissa and the direction of the resulting force F was determined (fig. 3).

A simple approach was made for the extrapolation of the pressure towards the leading and trailing edges. The pressure at the leading edge was estimated by averaging the pressure values at the 10% chord positions on PS and SS, while the pressure at the trailing edge was determined by averaging the pressures at the 90% chord positions. Certainly this approach is only nearly correct for design conditions, when the stagnation points are very close to the leading edge and trailing edge, respectively. To verify the approach the extrapolated pressure distribution of the piezoresistive sensors was compared with the results of the pressure taps. The pressure taps had a minimum distance of only 2.5% chord length from the leading edge and trailing edge, respectively. This comparison was done for several stable operating points between design point and stability limit. In every case the extrapolated pressures from the piezoresistive sensors are in good consistence with the measured values of the pressure taps near the leading edge and trailing edge, respectively.

For operating points close to the stability limit the point of maximum loading is shifted towards the leading edge of the blades. Using the extrapolation the pressures between leading edge and the first sensor positions on the PS and SS are possibly under- or overestimated. Indeed it was verified for the investigated blades, that these errors are nearly compensated when calculating the dominant force component F_y by integrating the pressure distribution. On the other hand the force component F_x would clearly be underestimated if the extrapolation would not been used. This is because of the fact, that the largest portion of this force component is induced near the leading edge and the trailing edge. The tests therefore confirmed, that the extrapolation improves the accuracy of the force calculation from the measured pressure distributions. Eventually the recent numerical investigations of Jia et al. [12] showed a good agreement of the time-averaged and the time-resolved blade pressure forces with the experimental results.

A restriction of the experimental setup is that local changes of the time-resolved pressure at the leading or trailing edge can certainly not be realized with the extrapolation. These changes can possibly appear due to small separation bubbles during rotating stall operation, for instance. Furthermore the spanwise variation of the unsteady aerodynamic force can not be determined with the current experimental setup. However, it is pointed out by other researchers, that there are no major radial variations of the full-span RS structure (e.g. Palomba et al. [13]). Thus we can regard the pressure forces determined at the midspan as a good approximation for the pressure forces of the whole blade.

The sampling rate for the measurements was set to 32.77 kHz. The pressure force calculation is done for each individual time step of the measuring data. No averaging of the data is done. The rotor blade passing frequency (BPF) is 1.05 kHz for design speed. Viewed from the rotating frame of reference the passing frequencies of the stator blades and the IGV's are 1.38 kHz and 0.85 kHz, respectively. Thus the blade passing signals are well resolved. As a result, the time-resolved pressure force parameters for a single rotor and a single stator blade are obtained. The contribution of shear forces to the overall aerodynamic blade force can not be taken into account.

Eventually, the data obtained with two casing-mounted piezoresistive pressure sensors (*Kulite XT190*) were used to discuss the stall inception and development process.

3 STALL INCEPTION PROCESS AND FUNDAMENTAL STALL CELL STRUCTURE

The stability behavior of the Dresden LSRC was extensively investigated by Mailach [5]. A short summary of this previous work will be provided below to give insight into

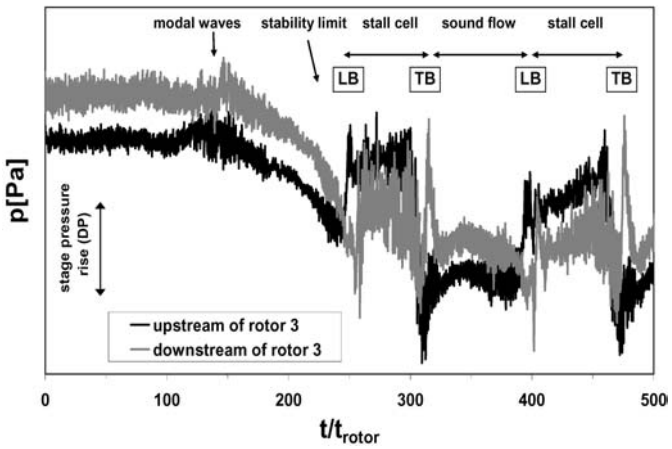

Fig. 4: Casing wall pressure within axial gaps up- and downstream of rotor 3

the flow structure at the stability limit and during RS operation. As an example the stall inception in the third compressor stage is shown in fig. 4. In this diagram the casing wall pressures in the middle of the axial gaps up- and downstream of the rotor blade row are presented. The arbitrary time scale is related to the rotor blade passing period t_{rotor}.

Two independent modal waves can be found in the stable operating range of the Dresden LSRC. The modal disturbances can be described by the 1. and 2. mode order. This corresponds to a circumferential wavelength of 360 degrees and 180 degrees, respectively. The modal waves are associated with wavelike variations of the flow properties (pressure, velocity, blade incidence etc.) and propagate in circumferential and axial direction. Axially reversed flow does not appear due to the disturbances [5]. The circumferential propagation speed of the two different modal waves is about 25-30%, but differs from each other.

Just before the stability limit the two modal waves superimpose, while their amplitudes increase. In fig. 4 the last appearance of the modal waves can be seen in the time period t/t_{rotor}=120-160. They can be identified by a rise of the pressure and its fluctuations. Simultaneously the blade incidence increases until the critical incidence angle of the blading is exceeded. As a result of this a single-cell full-span RS develops directly from the modal waves in the first compressor stage. From there it expands very fast to all compressor stages. In fig. 4 a rapid pressure drop indicates that stall is reached (t/t_{rotor}=160-250). Surge does not appear in the Dresden LSRC, because of the comparably low flow velocities and the small downstream plenum.

At about t/t_{rotor}=250 the stall cell arrives the considered measuring positions in the third stage (fig. 4). This boundary of the stall cell is denoted as leading boundary (LB). Within the stall cell the axial velocity component is negative (deep stall). The fluid is therefore transported from the compressor exit towards the inlet. This is verified by the results of hot-wire measurements [5]. The mean pressure level as well as the pressure fluctuations within the stall cell are higher than in the region of sound flow between the cells (fig. 4).

At the trailing boundary of the stall cell (TB) the flow changes from stalled to unstalled condition. The subsequent period with sound flow is visible between t/t_{rotor}=320-390. The sound forward flow shows comparable characteristics to the flow field of the normally operating compressor, but at a lower pressure level. This is in accordance to the observations of Palomba et al. [13].

At t/t_{rotor}=390 the stall cell appears again at the considered measuring position. After this first revolution of the stall cell it is already fully developed and does not change its size, pattern and circumferential speed remarkably. The stalled flow region covers about 160 degrees of the circumference. For design speed the stall cell rotates 6.5 times per second with respect to the fixed frame (40% of rotor turning speed) and about 10 times per second with respect to the rotating frame of reference (60% of rotor speed).

An important characteristic during RS operation are the pressure peaks and valleys appearing at the cell boundaries (LB and TB, fig. 4). This feature has already been observed by Cumpsty and Greitzer [14], Gyarmathy [15] and Saxer-Felici et al. [16]. It is discussed by those authors that the fluid inertia is responsible for a momentum exchange of the fluid of adjacent blade rows at the stall cell boundaries.

The stall cell moves relatively to both the fixed and the rotating frame of reference with a velocity below the rotor speed. Therefore at the TB of the cell the flow within the rotor blade channels changes from unstalled to stalled flow condition, while in the stator blade channels the flow is going from stalled to unstalled. Due to the fluid inertia the sound flow within the rotor blade channels meets the stagnant flow within the stator blade channels for a short duration at the TB of the stall cell. According to Cumpsty and Greitzer [14] this inertia effect concerns only one or two blade channels. So the flow through the rotor blade channels changes very fast from a large velocity to near zero or even axially reversed flow at the considered TB of the stall cell. This results in a local positive peak of the pressure rise across the rotor blade row and a negative one across the stator blade rows. In other words, at the TB a sharp pressure drop (valley) can be found in the axial gap upstream of a rotor blade row and a sharp pressure increase (peak) appears downstream of the rotor blade row.

At the LB of the cell the opposite effect appears, since the flow within the rotor blade channels changes from stalled to unstalled flow condition, while in the stator blade channels the flow is going from unstalled to stall. As a result of this at the LB a sharp pressure peak can be found upstream of the rotor blade row and a distinct pressure valley downstream of it. These observations are confirmed by the work of Gyarmathy [15], who further improved the understanding of the momentum exchange process at the stall cell boundaries. The role of this momentum exchange on the stall cell propagation is clearly pointed out there. The appearance of these pressure peaks in a single-stage axial compressor is confirmed by Saxer-Felici et al. [16].

Clear signs of this momentum exchange process at the stall cell boundaries can also be observed in the Dresden LSRC (fig. 4). At the cell boundaries (LB and TB) spiky pressure peaks and valleys appear. Upstream of the rotor blade row a pressure peak at the LB and a pressure valley at the TB are dominant. Downstream of the considered rotor blade row the opposite pressure excursions can be found at the cell boundaries. This generally confirms the observations in refs. [14], [15] and [16].

Indeed these pressure excursions due to the momentum exchange are superimposed on the fundamental flow field, which is determined by the influence of the wakes and the potential effects of the blades. Therefore the momentum exchange effects can be masked sometimes. Furthermore in a multistage compressor an aerodynamic interaction of several up- and downstream blade rows takes place, which makes the flow field much more complex. So the different pressure peaks in the time-resolved data in fig. 4 can not clearly be interpreted in every case. Anyway, several pressure peaks and valleys can be identified at the cell boundaries and will have a remarkable influence on the unsteady pressure forces of the blades. In contrast to the assumptions of Cumpsty and Greitzer [14] the strong peaks due to the momentum exchange covers not only one or two blade passages but a larger circumferential flow region corresponding to a maximum of 10-15 passing blades (fig. 4, LB and TB of stall cell).

As discussed by Cumpsty and Greitzer [14] the axial velocity discontinuity at the LB is less abrupt than at the TB of the stall cell. As a result the peaks at the TB are more evident. Gyarmathy [15] observed the same tendency. This trend is also confirmed by our results. It can be seen in fig. 4 that the peak-to-peak value of the pressure signals up- and downstream of the rotor blade row is clearly larger at the TB than at the LB. The short-duration pressure difference at the TB of the cell has the order of magnitude of up to 2-times of the compressor stage pressure rise.

In the next section the influence of the observed flow patterns on the unsteady pressure forces on the rotor and stator blades of the first stage will be discussed.

4 TIME-RESOLVED BLADE PRESSURE FORCES AT THE STABILITY LIMIT AND DURING ROTATING STALL

Stator 1

Figure 5 shows the results of the time-resolved pressure force calculations at midspan of stator 1 at the stability limit and during RS. In these diagrams the time is related to the rotor blade passing period t_{rotor} (identical rotor blade number in all stages). A period of 700 rotor blade passings is shown, which corresponds to about 0.67 seconds and 11.1 rotor revolutions, respectively.

For comparison the time-resolved pressure on PS and SS at 50% chord at midspan are depicted in fig. 5a. The profile pressures on stator 1 show a qualitatively comparable behavior like the casing wall pressures discussed by means of fig. 4. The modal wave influence is stronger in the first stage and leads there to the RS inception, denoted as stability limit in fig. 5a. Subsequently the change between stalled and sound flow is indicated by these data. The momentum exchange process at the cell boundaries, discussed in the previous section, has obviously also a strong influence on the profile pressures. The pressure excursions at the stall cell boundaries are clearly to be seen in fig. 5a. Furthermore both before and after the stability limit the passing blades are responsible for high-frequency fluctuations of the profile pressures.

Fig. 5b shows the resulting blade pressure force. It seems not to be useful to relate the force to its mean value of the considered time period or to calculate a force coefficient, since after passing the stability limit a permanent change between sound and stalled flow appears at the blade considered. For comparison the time-resolved force is therefore related to the absolute value of the mean pressure force at design point (DP) of the compressor. The mean coefficients of force, force components and torque for the design point are given in ref. [8].

In figs. 5c-e the force components and the torque are depicted. These parameters are again related to its absolute mean value at DP. So the sign of this related force components and the force component itself is identical. (Please note, that the mean F_x and M_{CG} are negative at DP). Furthermore fig. 5f shows the angle between the blade chord direction and the resulting force F. The definitions of these parameters are given in fig. 3.

To show the details at the most interesting points of time, 8 shorter time periods (5 rotor blade passings) are marked in fig. 5c and depicted in separate diagrams (fig. 5g/1-8). The ordinate of the left diagram is valid for all diagrams in fig. 5g. The parameter considered is the dominating force component F_y. The amount of this component is nearly identical to that of the resulting force F because of the small contribution of F_x. However, it is useful to consider F_y instead of F in more detail, since it additionally indicates the change of the flow direction.

The main source of unsteadiness of the profile pressures and the blade pressure forces within the stable operating range are rotor-stator-interactions due to the viscous wakes and the potential effects of the blades. For the Dresden LSRC this topic is extensively discussed by Mailach et al. [7], [8].

Approaching the stability limit the influence of the long-lengthscale modal waves on the excited force increases (fig. 5b). The low-frequency influence of the modal waves superimposes to the high-frequency wake and potential effects. Already for stable operating points near the stability limit the amplitudes of the low frequency modal waves can be in the same order of magnitude as those of the fluctuations with the BPF's (compare fig. 7 in Mailach and Vogeler [8]).

It becomes obvious at points 1-3 (figs. 5c and 5g/1-3), that substantial differences of the blade excitation arise from the superposition of the blade passing events and the modal waves. At point 1 the fluctuations due to the blade passing are somewhat increased compared to stable operating points. The peak-to-peak value is now about +/- 40%, while this value was

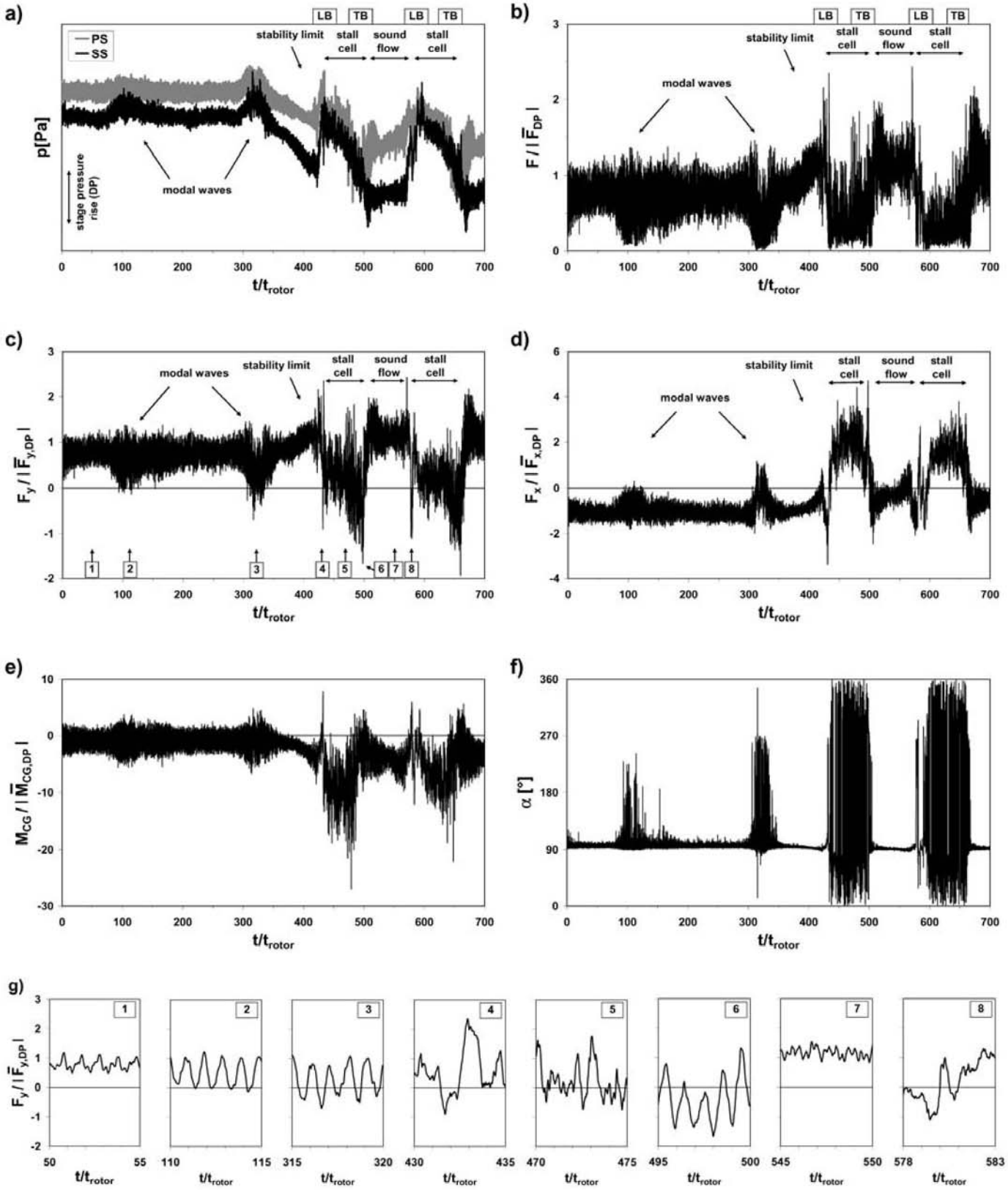

Fig. 5: Stator 1: profile pressures at 50% chord and blade pressure force parameters at the stability limit and during rotating stall (midspan, design speed)

at the most +/-35% for stable operating points [8]. However, at points 2 and 3 the stator blade under consideration is inside a region of larger blade incidence provoked by the long-lengthscale modal waves. As a result of this a remarkable increase of the fluctuation amplitudes of the blade pressure force can be observed. At point 2 the force F and its dominant component F_y periodically changes between maximum values of up to 130% and zero. This process is triggered with the passing rotor blades. During the last revolution of the modal waves its influence further increases (point 3, fig. 5g/3). Pulsed by the rotor blade passing now the force components F_y and F_x changes between positive and negative values with very large amplitudes. This is probably the first sign of the short-duration appearance of flow separations (axially reversed flow) leading to RS inception during the next revolution of the modal waves. As a result the force angle of attack α very strongly changes between 90 and 270 degrees during the last appearance of the modal waves (about t/t_{rotor}=310-340 in fig. 5f). That means the "normal" direction of the resulting force from PS towards the SS is changing to the opposite direction and back for each passing rotor blade.

After the last passing of the modal wave a rotating stall cell develops directly from it. Because of the blockage of the growing stall cell the flow is turned into circumferential direction. Just before the first appearance of the stall cell this leads to a higher blade incidence and consequently an increase of the blade pressure force at the stator blade considered (fig. 5b,c).

The stability limit is reached at about t/t_{rotor}=420-430 (LB of first stall cell appearance). An extreme increase of the force amplitudes appears at this transition point from the stable flow regime to the reversed flow region of RS. Spiky fluctuations of the force parameter can be found due to the momentum exchange process between the blade rows, discussed before. The peak amplitudes of the force F are up to nearly 250% of the mean force at DP. The force fluctuations show a stochastic pattern, the influence of the passing blades is not dominant at the stall inception point (figs. 5b and 5g/4).

The first passing of the stall cell, which is coupled with axial reversed flow, appears between t/t_{rotor}=430-500. The mean values of the force F within the stall cell are somewhat below those just before the stability limit. Considerable fluctuations of the force and its direction occur with high frequencies. However, stochastic events predominate versus the periodic signal of the rotor blade passing. The component F_y strongly fluctuates between positive and negative values (figs. 5c and 5g/5). Furthermore the force direction strongly fluctuates within the stall cell, which points out the high unsteady mechanical loading of the blades (fig. 5f). The component F_x is positive due to the axial reversed flow within the stall cell (fig. 5d). Also the turning moment around the centre of gravity strongly fluctuates (fig. 5e). This can be explained by the fluctuations of the force as well as the strong shift of the centre of lift along the blade chord.

At the TB of the stall cell the flow conditions change from axial reversed to forward flow. The strong periodic changes of the pressure forces are linked to the effect of the passing blades, leading to a high amplitude aerodynamic blade excitation (fig. 5g/6). This is an explicit difference to the behavior at the LB and within the stall cell (compare to fig. 5g, points 4 and 5). The momentum exchange process at the considered TB – superimposed with the blade passing events – covers a time period of about 10-15 passing rotor blades (only a part of it is visible in fig. 5g/6). The amplitudes of the fluctuations due to the passing blades at the TB are much larger than in the stable operating range (compare to fig. 5g, points 1 and 2).

After the passing of the cell the blade under consideration is located in an area of sound forward flow (fig. 5, t/t_{rotor}=520-570 and fig. 5g/7). The mean aerodynamic force is in the same order of magnitude than for stable operating points. Also the fluctuations are low compared to those within the stall cell and especially at the stall cell boundaries.

At t/t_{rotor}=570 the LB of the stall cell again arrives the blade considered (e.g. fig. 5g/8). In accordance to the first appearance of the cell (LB, identical to stability limit), the fluctuations covers only a few blade passages and appears more stochastically than at the TB of the cell.

Rotor 1

The data for rotor 1 are presented in figs. 6a-g in the same way as for stator 1 (compare fig. 5). In the stable operating range the unsteady pressure force of rotor 1 is dominated by the potential effects of the downstream stator blades, which move relatively to the rotor blades considered [8]. The IGV wakes play only a secondary role. This is why the time-base in fig. 6 is referred to the passing period of the downstream stator blades t_{stator} in all cases. The dominance of the stator potential flow field propagating upstream on the unsteady pressure force excitation of rotor 1 is obvious in figs. 6g, points 1-3.

As already discussed for stator 1 the modal waves are responsible for a periodical change of the flow properties covering a larger sector of the circumference. The influence of this disturbance just before the stability limit can clearly be seen in the traces of the profile pressures and the force parameters of the rotor blades, depicted in fig. 6. The passing of the modal waves at a given position again leads to a modulation of the pressure force amplitudes due to the passing blades. The rotor blade considered is located in a region of larger incidence due to the modal waves at the points of time 2 and 3 (figs. 6g/2 and 6g/3). As a result a significant increase of the peak-to-peak amplitudes due to the stator blade potential effect appears (compared to point 1 for instance, fig. 6g/1). The main features of the discussed parameters before the stability limit are comparable for rotor 1 and stator 1.

The stability limit is indicated by a sharp pressure force peak visible at t/t_{rotor}=380-385 in fig. 6. At this point of time the force increases very fast to about 2.5-times of the design value (fig. 6g/4). The slip of the stall cell compared to the rotor turning velocity leads to a stall cell propagation within the relative frame opposite to the rotor turning direction itself.

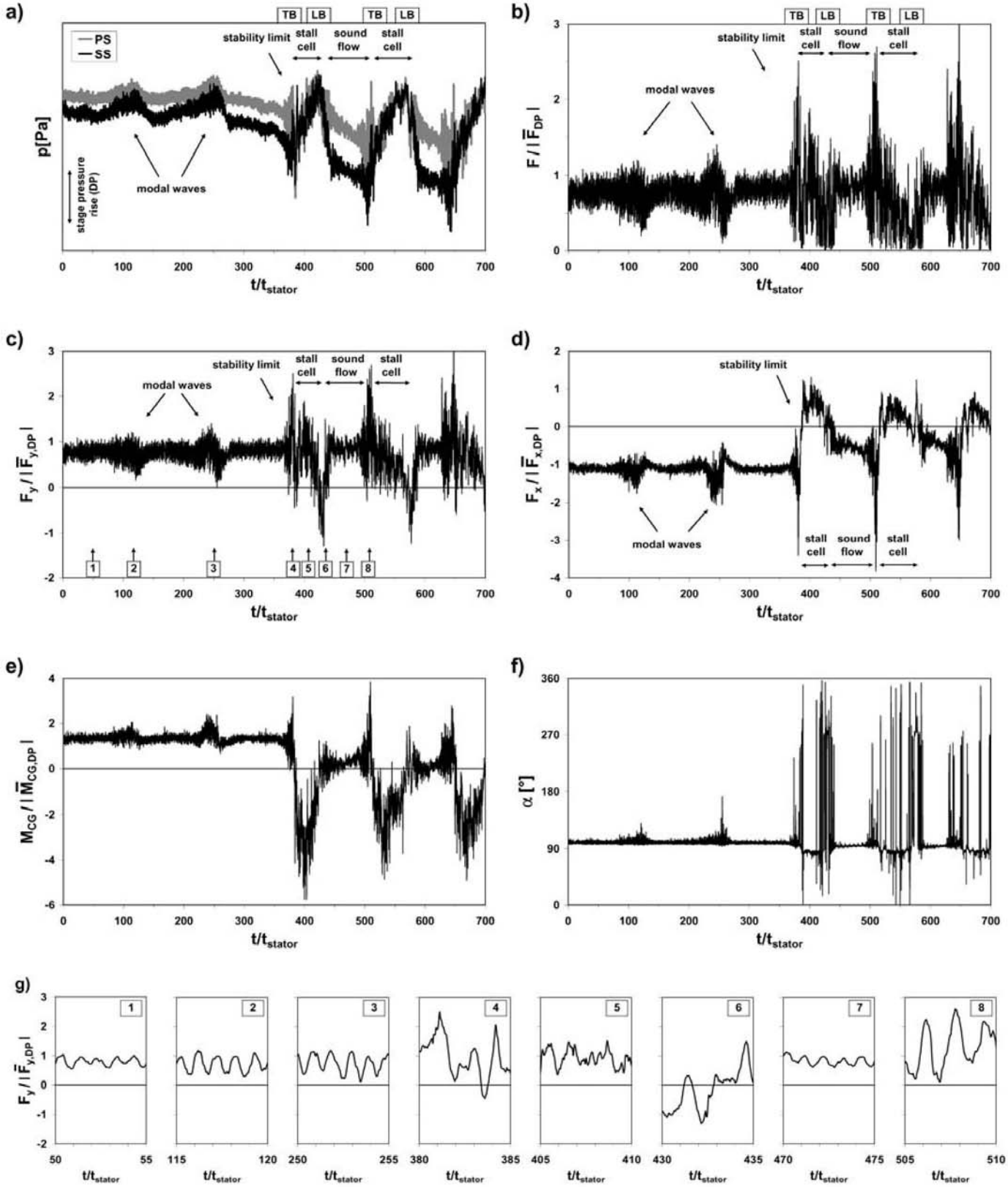

Fig. 6: Rotor 1: profile pressures at 50% chord and blade pressure force parameters at the stability limit and during rotating stall (midspan, design speed)

Thus the rotor blades traverse the stall cell in opposite direction than the stator blades. This can be seen in figs. 5a and 6a, for example in the signals of the sensors on the SS during the first cell passing: The stator blades enter the cell at the LB, after that the pressure decreases during cell passing and finally the stator blades leave the stall cell at the TB. In contrast the rotor blades enter the cell at the TB, after that the pressure increases until the rotor blades leave the cell at the LB.

The change between stalled and unstalled flow is indicated by the rotor blade force parameters in a qualitatively comparable form like for the stator blades (figs. 6b-f). As already discussed for stator 1, the maximum force fluctuations during the RS operation appear at the stall cell boundaries. Although the rotor blades traverse the stall cell in opposite direction than the stator blades the same fundamental features can be observed at the cell boundaries: these are high-amplitude fluctuations with the frequency of the passing blades at the TB and a more diffuse change of the flow properties at the LB (fig. 6).

At the stall cell boundaries - especially at the TB - the IGV passing is responsible for high-frequency large-amplitude pressure force fluctuations (fig. 6g/8). This points out the different flow mechanism at the cell boundaries compared to the behaviour within the stall cell and the region of sound flow between the cells. In these flow regions (as well as during stable compressor operation) the IGV passing plays only a minor role for the unsteady blade excitation.

The mean force during axial reversed flow within the cell is again comparable to that for the sound flow before stall inception (figs. 6b, 6c and 6g/5). However, the fluctuations of the pressure force are stronger during reversed flow conditions. As already observed for the stator blades stochastic fluctuations dominate within the stall cell. An indication of the reversal of the flow direction is again given by the change of the sign of the F_x-component (fig. 6d).

For the sound flow conditions outside the stall cell the potential effect of the downstream stator blades periodically changes the unsteady profile pressure distribution and consequently the blade pressure forces (e.g. fig. 6g/7). The IGV blade passing events are not visible. This is a comparable behaviour than observed before the stability limit (e.g. fig. 6g/1).

Thus a comparable development of the unsteady blade pressure forces concerning its fundamental features and amplitudes can be found on the rotor and stator blades at the stability limit and during RS.

5 FREQUENCY CONTENTS OF BLADE PRESSURE FORCES DURING ROTATING STALL

In the following the frequency contents of the aerodynamic blade forces during RS will be discussed. (Appropriate results for a stable operating point near the stability limit can be found in [8]). A consideration of the periodic portions of the force is useful for an estimation of the excited blade vibrations and a comparison to the natural frequencies of the blades. The frequency spectra of the force at the stator 1 and rotor 1 blades are shown in figs. 7a and 7b. For comparison the force is again divided by the mean pressure force at DP.

In both cases the dominant influence on the unsteady blade pressure forces appears due to the stall cell. The single stall cell propagates with 40% of rotor turning speed in the fixed frame and 60% of rotor speed with respect to the rotor blades. This leads to a RS-frequency of f_{RS}=6.5 Hz on the stator blade and f_{RS}=10.0 Hz on the rotor blades (marked with circles in fig. 7). Several higher harmonics of the RS-frequency are visible in both cases because of the complex RS-structure. Especially on the rotor blades these multiples of the fundamental RS-frequency covers a large frequency range of up to 140 Hz (14^{th} harmonic of f_{RS}), fig. 7b. However, this upper frequency is clearly below the first natural frequencies of the blades (first bending mode at 200 Hz, first torsion mode at 440 Hz).

The BPF's of the IGV and the stator appears on the rotor blades at 850 Hz and 1380 Hz, respectively (fig 7b). Both frequencies are modulated with the RS-frequency, leading to a broad band aerodynamic blade excitation. Although the IGV passing is only dominant during the short time periods at the stall cell boundaries (especially at the TB, compare fig. 6g/8), the amplitudes in the frequency spectrum are somewhat higher than those due to the downstream located stator blade. This is in contrast to the observations for stable operating points, where the upstream potential influence of the stator blades was much stronger than that of the IGV wakes (fig. 6g/1, more

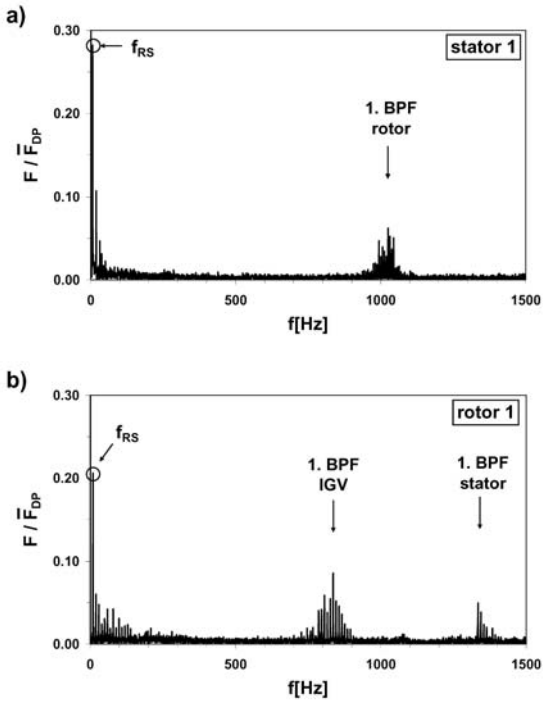

Fig. 7: Frequency spectra of pressure force at stator and rotor blades during rotating stall (first stage, midspan, design speed)

details in [8]). Higher harmonics of the BPF's are of less influence.

On the stator blades the rotor BPF is again modulated with the RS-frequency (fig. 7a). Because of the same rotor blade numbers in all stages the effects from up- and downstream can not be distinguished in this case.

Since the frequency spectra are reflecting periodic events, the amplitudes at the frequencies, which can be attributed to the RS-cell and the blade passing, are clearly lower than visible in the time-resolved force traces (compare for instance to figs. 5b and 6b). This is also due to the fact that the flow structure during RS permanently changes between stalled and unstalled flow. Thus the dominating effects and their amplitudes always change and they are not strongly periodic for the time period used to determine the frequency spectra.

6 CONCLUSIONS

In this paper experimental investigations of the unsteady aerodynamic blade excitation in the Dresden four-stage low-speed compressor are presented. Results are shown for the rotor and stator blades of the first stage for operating conditions at the stability limit and during rotating stall. To the best knowledge of the authors these are the first experimental data on time-resolved blade pressure forces for rotating stall operation in axial compressors, available in open literature.

The stall inception process and the fundamental features of the stall cell structure and propagation are discussed. It was found, that rotor-stator-interactions play an important role on the aerodynamic blade force excitation for stable compressor operation as well as during rotating stall. Just before the stability limit modal waves are responsible for low-frequency fluctuations of the unsteady profile pressures and the pressure forces with comparable large amplitude. The modal wave influence superimposes to the high-frequency blade passing events. This leads to a periodic change of the unsteady blade excitation amplitudes.

A single-cell full-span rotating stall cell directly develops from the modal waves. At the stall inception point a strong short-duration increase of the blade pressure forces appears. Within the stall cell large stochastic fluctuations of the blade pressure forces and its direction have been found. For sound flow conditions outside the stall cell a comparable development of the time-resolved blade pressure forces like for stable operating points have been observed.

The theory of the momentum exchange between adjacent blade rows at the stall cell boundaries, where the stalled und the sound flow meets for short time durations, is confirmed by the presented investigations. Due to the momentum exchange the maximum blade pressure force fluctuations appear at the stall cell boundaries. New features found for the momentum exchange process are, that it covers several blade passing events and is triggered by the passing blades. Especially at the trailing boundary of the stall cell the blade passing plays a dominant role for the aerodynamic blade excitation. The peak force amplitudes during rotating stall operation amount to 2.5-times of the mean force at design point.

The frequency spectra of the blade pressure forces are dominated by the rotating stall frequency and its harmonics. Further periodic force fluctuations appear with the blade passing frequencies of the adjacent blade rows, which are modulated with the rotating stall frequency.

ACKNOWLEDGMENTS

The work reported in this paper was performed within the project "Unsteady Forces and Boundary Layer Behaviour on the Blades of a Low-Speed Axial Compressor" which is part of the joint project "Periodical Unsteady Flow in Turbomachines" funded by the Deutsche Forschungsgemeinschaft (DFG, German Research Society).

NOMENCLATURE

f	[Hz]	frequency
F	[N]	blade pressure force
l	[m]	chord length
M	[Nm]	torque
p	[Pa]	pressure
t	[s]	time
x	[m]	chordwise position
y	[m]	position perpendicular to chord
α	[deg]	angle between resulting force and tangent at the profile contour (x-direction), see fig. 3
$\bar{}$		mean value

Abbreviations and Subscripts

BPF	blade passing frequency
CG	centre of gravity
CL	centre of lift
DP	design point
IGV	inlet guide vane
LB	leading boundary of the stall cell
LSRC	Low-Speed Research Compressor
MS	midspan
PS	pressure side
RS	rotating stall
SS	suction side
TB	trailing boundary of the stall cell
x	component in blade chord direction
y	component perpendicular to the blade chord

REFERENCES

[1] McDougall, N. M., Cumpsty, N. A., Hynes, T. P., 1990: "Stall Inception in Axial Compressors", ASME Journal of Turbomachinery, Vol. 112, pp. 116-125.

[2] Day, I. J., Breuer, T., Escuret, J., Cherett, M., Wilson, A., 1999: "Stall Inception and the Prospects for Active Control in Four High-Speed Compressors", ASME Journal of Turbomachinery, Vol. 121, pp. 18-27.

[3] Höss, B., Leinhos, D., Fottner, L., 2000: "Stall Inception in the Compressor System of a Turbofan Engine", ASME Journal of Turbomachinery, Vol. 122, pp. 32-44.

[4] Camp, T.R., Day, I.J., 1998: “A Study of Spike and Modal Stall Phenomena in a Low-Speed Axial Compressor”, ASME Journal of Turbomachinery, Vol. 120, pp. 393-401.

[5] Mailach, R., 2001: „Experimentelle Untersuchung von Strömungsinstabilitäten im Betriebsbereich zwischen Auslegungspunkt und Stabilitätsgrenze eines vierstufigen Niedergeschwindigkeits-Axial-verdichters“, PhD thesis, TU Dresden, Fortschritt-Berichte VDI, Reihe 7, Nr. 410, VDI-Verlag, Düsseldorf, Germany.

[6] Mailach, R., Lehmann, I., Vogeler, K., 2001: „Rotating Instabilities in an Axial Compressor Originating from the Fluctuating Blade Tip Vortex“, ASME Journal of Turbomachinery, Vol. 123, pp. 453-463.

[7] Mailach, R., Vogeler, K., 2004: “Rotor-Stator Interactions in a Four-Stage Low-Speed Axial Compressor, Part I: Unsteady Profile Pressures and the Effect of Clocking”, ASME Journal of Turbomachinery, Vol. 126, pp. 507-518.

[8] Mailach, R., Müller, L., Vogeler, K., 2004: “Rotor-Stator Interactions in a Four-Stage Low-Speed Axial Compressor, Part II: Unsteady Aerodynamic Forces of Rotor and Stator Blades”, ASME Journal of Turbomachinery, Vol. 126, pp. 519-526.

[9] Sauer, H., Bernstein, W., Bernhard, H., Biesinger, T., Boos, P., Möckel, H., 1996: „Konstruktion, Fertigung und Aufbau eines Verdichterprüfstandes und Aufnahme des Versuchsbetriebes an einem Niedergeschwindigkeits-Axialverdichter in Dresden“, Abschlußbericht zum BMBF-Vorhaben 0326758A, Dresden, Germany.

[10] Müller, R., Mailach, R., Lehmann, I., 1997: “The Design and Construction of a Four-Stage Low-Speed Research Compressor”, in: Badur, J., Bilicki, Z., Mikielewicz, J., Sliwicki, E. (eds.), Proceedings of the IMP ’97 Conference on Modelling and Design in Fluid-Flow Machinery, pp. 523-530, Gdansk, Poland, Nov. 18-21, 1997.

[11] Boos, P., Möckel, H., Henne, J.M., Selmeier, R., 1998: “Flow Measurement in a Multistage Large Scale Low Speed Axial Flow Research Compressor”, ASME paper 98-GT-432.

[12] Jia, H., Vogeler, K., Müller, L., Mailach, R., 2006: „Numerical Investigation of Rotor-Stator-Interactions in a 1.5-Stage Low-Speed Axial Compressor“, Conference on Modelling Fluid Flow (CMFF'06), Budapest, Hungary, Sept. 6-9, 2006, to be published.

[13] Palomba, C., Puddu, P., Nurzia, F., 2003: “Experimental Investigation of Rotating Stall Cell Structure Variation During Recovery”, in: Stastny, M., Sieverding, C. H., Bois, G. (eds.), Proceedings of the 5th European Conference on Turbomachinery - Fluid Dynamics and Thermodynamics, pp. 187-195, Prague, Czech Republic, March 18-21, 2003.

[14] Cumpsty, N.A., Greitzer, E.M., 1982: “A Simple Model for Compressor Stall Cell Propagation”, Transactions of the ASME, Journal of Engineering for Power, Vol. 104, pp. 170-176.

[15] Gyarmathy, G., 1996: “Impeller-Diffuser Momentum Exchange During Rotating Stall”, ASME paper 96-WA/PID-6.

[16] Saxer-Felici, H.M., Saxer, A.P., Inderbitzin, A., Gyarmathy, G., 1999: “Prediction and Measurement of Rotating Stall Cells in an Axial Compressor”, ASME Journal of Turbomachinery, Vol. 121, pp. 365-375.